International Compressor Engineering Conference   School of Mechanical Engineering

1990

Dynamic Analysis of a Rotor-Journal Bearing System for Twin Rotary Compressors

H. Hattori
Toshiba Corporation

N. Kawashima
Toshiba Corporation

Dynamic Analysis of a Rotor-Journal Bearing System
for Twin Rotary Compressors

Hitoshi HATTORI, Noritsugu KAWASHIMA

Mechanical Engineering Laboratory

R&D Center, Toshiba Corporation

ADDRESS : 4-1, Ukishima-cho, Kawasaki-ku, Kawasaki 210, Japan

ABSTRACT

A rotor-journal bearing system for a twin rotary compressor has been numerically analyzed to estimate the reliability and to optimize the bearing design. For rotary compressors, large dynamic loads act on the rotor. They are unbalanced forces due to eccentric rotation parts and gas forces induced by the difference in pressure between compression and suction gases. In such a case, the rotor-journal bearing system becomes nonlinear, because the stiffness and damping coefficients of the lubricating oil film in the bearings vary. Such a rotor system is solved as a coupled problem of momentum equations and Reynolds equations for all the bearings. The analytical procedure and the results are described in this paper.

INTRODUCTION

Twin rotary compressors have double compression units. Two rolling pistons mounted on the rotor have eccentricity in the opposite direction with each other. Torque fluctuations are smaller than those of single rotary compressors because gas is compressed twice per rotor revolution. So, they have the advantages of low noise and low vibration. The authors have developed a twin rotary compressor for air conditioners. It is able to be operated from 15 Hz to 150 Hz in rotating frequency against 30 Hz to 150 Hz for single rotary compressors. Therefore, the capacity of the air conditioner can be varied more widely.

In general, large dynamic loads act on the rotor of rotary compressors. They are unbalanced forces due to the eccentric rotation of the rolling pistons and the balancers, and gas forces induced by the difference in pressure between compression and suction gases. Therefore, when the compressor is driven at high speed, the rotor rotates with a large bending deformation, and the journal bearings are put under a severe condition. Such a rotor-journal bearing system has been numerically analyzed for the above-mentioned twin rotary compressor. It is important to investigate the rotor action and the bearing load characteristics

to estimate the reliability of the rotor system and to optimally design the bearing. The analytical procedure is described and the results are discussed as compared with those of the single rotary compressor.

GOVERNMENT EQUATIONS

Fig.1 shows the rotor-journal bearing system of a twin rotary compressor and its coordinate system for analysis. An elastic flexible rotor is supported by three journal bearings S_{B1}, S_{B2} and S_{B3} approximated by the short bearing theory. In the rotor system, it must be considered that the stiffness and damping coefficients of the oil film in the bearings vary due to large dynamic loads, namely, unbalanced forces and the gas forces. Therefore, the Reynolds equations are used to calculate the bearing reaction forces.

Momentum Equations of a Rotor

The momentum equations of an elastic flexible rotor are partial differential equations. In this analysis, they are exchanged with ordinary differential equations by the finite element method. Using one-dimensional beam elements which have a local coordinate system shown in Fig.2, the inertia and stiffness terms of the elements are written as follows in x,y directions, respectively. Subscript e displays that individual matrices[1] and vectors are element units.

$$
\begin{array}{lll}
& \underline{\text{x-direction}} & \underline{\text{y-direction}} \\
\text{Inertia terms} \quad : & m\,[M_x]_e\,\{\bar{x}\}_e & m\,[M_y]_e\,\{\bar{y}\}_e \qquad (1)
\end{array}
$$

$$
\text{Stiffness terms} : EI\,[K_x]_e\,\{x\}_e \qquad EI\,[K_y]_e\,\{y\}_e \qquad (2)
$$

$$
\{x\}_e = [x_n,\ \alpha_n,\ x_{n+1},\ \alpha_{n+1}]^T_e \qquad \{y\}_e = [y_n,\ \beta_n,\ y_{n+1},\ \beta_{n+1}]^T_e \qquad (3)
$$

where $m = \rho\,A\,l$, m is the mass, ρ is the density, A is the cross section, l is the length, and EI is the flexural stiffness (E is Young's modulus, I is the second moment of area) of the elements, respectively, and x_n and y_n are the deflections of the node n in the x,y directions, and α_n and β_n are the rotations of the node n around the y and x axes, respectively. Considering the inertia of rotation for the motor rotor overhanging from the upper bearing, the mass matrices are

$$
[M_x]_e = [M_{ox}]_e + k_d^2[M_{ix}]_e \qquad [M_y]_e = [M_{oy}]_e + k_d^2[M_{iy}]_e \qquad (4)
$$

$$
k_d^2 = (d_o^2 + d_i^2)/16 \qquad (5)
$$

where d_o is the outer diameter and d_i is the inner diameter of the elements. The momentum equations of a system matrix form for the elastic flexible rotor are

derived by assembling the element matrices and the element vectors.

$$[M_x]\{\ddot{x}\} + [K_x]\{x\} - \{F_{Bx}(x,y,\dot{x},\dot{y})\} = \{F_x\}$$

(6)

$$[M_y]\{\ddot{y}\} + [K_y]\{y\} - \{F_{By}(x,y,\dot{x},\dot{y})\} = \{F_y\}$$

$$\{x\} = [x_1, \alpha_1, x_2, \alpha_2, \ldots, x_n, \alpha_n, \ldots, x_N, \alpha_N]^T$$

(7)

$$\{y\} = [y_1, \beta_1, y_2, \beta_2, \ldots, y_n, \beta_n, \ldots, y_N, \beta_N]^T$$

where $\{F_{Bx}\}$ and $\{F_{By}\}$ are the bearing reaction forces, and $\{F_x\}$ and $\{F_y\}$ are the outer loads acting on the rotor. The bearing reaction forces are given by integrating the oil pressure obtained by solving the Reynolds equations. They act on the nodes put on the bearings, and equal zero on the other nodes. The boundary condition of the rotor ends where $n = 1$ and N is the free end, automatically satisfied in the case of the finite element method.

Bearing Reaction Forces

The pressure gradient of the oil film in the circumferential direction can be ignored by the short bearing theory. Then, the reduced Reynolds equation is

$$\partial(h_i^3(\partial p_i/\partial z))/\partial z = 6\,\omega\,\mu_i(\partial h_i/\partial \theta) + 12\,\mu_i(\partial h_i/\partial t)$$

(8)

$$h_i = c_i - x_n \cos\theta - y_n \sin\theta$$

(9)

where i is the number of the bearings (here 1 to 3 for S_{B1}, S_{B2} and S_{B3}), p_i is the oil pressure, μ_i is the oil viscosity, c_i is the radial clearance, ω is the angular speed of rotation, and h_i is the oil film thickness. Differentiating Eq.(9) with t and θ,

$$(\partial h_i/\partial \theta) = x_n \sin\theta - y_n \cos\theta \qquad (\partial h_i/\partial t) = -\dot{x}_n \cos\theta - \dot{y}_n \sin\theta$$

(10)

Substituting Eqs.(9) and (10) into Eq.(8), and integrating under the boundary condition $p_i = p_a$ where $z = 0$, L_i, the pressure $p_i - p_a$ is obtained.

$$p_i - p_a = 3\,\mu_i z(z - L_i)\,f_p(\theta)$$

(11)

$$f_p(\theta) = [\omega(x_n \sin\theta - y_n \cos\theta) - 2(\dot{x}_n \cos\theta + \dot{y}_n \sin\theta)]$$

$$/(c_i - x_n \cos\theta - y_n \sin\theta)^3$$

(12)

where L_i is the bearing length. The bearing reaction forces F_{Bxi}, F_{Byi} are obtained by integrating Eq.(11).

$$
\left.\begin{array}{r} F_{Bxi} \\ F_{Byi} \end{array}\right\} = - R_{Bi} \int_0^{L_i} \int_{\theta 2}^{\theta 1} (p_i - p_a) \left\{\begin{array}{c} \cos\theta \\ \sin\theta \end{array}\right\} d\theta \, dz
$$

$$
= (1/2) \, R_{Bi} \, \mu_i \, L_i^{\ 3} \int_{\theta 2}^{\theta 1} f_p(\theta) \left\{\begin{array}{c} \cos\theta \\ \sin\theta \end{array}\right\} d\theta \tag{13}
$$

where R_{Bi} is the rotor radius, and θ_1 and θ_2 are the boundary conditions in the θ direction.

OUTER LOADS

Unbalanced Forces

Unbalanced forces due to the rolling pistons and the balancers rotate with the same speed as the rotor. The unbalanced forces are

$$
\left.\begin{array}{r} F_{uxj} \\ F_{uyj} \end{array}\right\} = (W_j/g) \, r_j^{\ 2} \omega \left\{\begin{array}{c} \cos(\psi + \phi_{uj}) \\ \sin(\psi + \phi_{uj}) \end{array}\right\} \tag{14}
$$

where, $j = 1, 2, \ldots, W_j$ is the eccentric weight, r_j is the eccentric radius, g is the gravitational acceleration, ψ is the rotor rotating angle shown in Fig.1 and ϕ_{uj} is the phase difference to ψ.

Gas Forces

Gas forces are induced by the difference in pressure $p(\psi)$ and ps between the two cells formed by the blade, as shown in Fig.1. They rotate with one half of ψ, and act on the rotor at the upper and lower compression units with a phase difference of 180°, with each other. The gas forces F_{Gx} and F_{Gy} are obtained by integrating the difference in $p(\psi)$ and ps along the side area of the rolling piston.

$$
\left.\begin{array}{r} F_{Gx}(\psi) \\ F_{Gy}(\psi) \end{array}\right\} = 2(p(\psi) - p_s) \, h_c \, R_r \, \sin(\phi/2) \left\{\begin{array}{c} \cos(\psi/2) \\ \sin(\psi/2) \end{array}\right\} \tag{15}
$$

where $\phi = 2\pi - \psi$, p_s is the suction pressure, h_c is the cylinder height, and R_r is the radius of the rolling piston. When the gas is adiabatically compressed from $\psi = 0°$, $p(\psi)$ is

$$
p(\psi) = \left\{ \begin{array}{ll} p_s \, (V_s/V(\psi))^{\gamma} & : p(\psi) < p_d \\ p_d & : p(\psi) \geq p_d \end{array}\right. \tag{16}
$$

where γ is the specific heat ratio, p_d is the discharge pressure, $V_s = V(0)$, and $V(\psi)$ is[2]

$$V(\psi) = (1/2) \, h_c \, R_c^2 \, f(\psi) \tag{17}$$

$$f(\psi) = (1-a^2) \, \phi - (1/2)(1-a)^2 \sin(2\phi) - a^2 \sin^{-1}\{(1/a-1)\sin\phi\}$$

$$-a(1-a)\sin\phi \, [1-\{(1/a-1)\sin\phi\}^2]^{1/2} \tag{18}$$

where $a = R_r/R_c$, and R_c is the inner radius of the cylinder.

ANALYTICAL PROCEDURE AND MODELS

Anlytical Procedure

Using the inverse matrices of the mass matrices $[M_x]$, $[M_y]$, equation(6) is deformed as follows.

$$\{\ddot{x}\} = [M_x]^{-1}(\{F_x\} + \{F_{Bx}(x,y,\dot{x},\dot{y})\} - [K_x]\{x\})$$
$$\{\ddot{y}\} = [M_y]^{-1}(\{F_y\} + \{F_{By}(x,y,\dot{x},\dot{y})\} - [K_y]\{y\}) \tag{19}$$

Outer loads $\{F_x\}$, $\{F_y\}$ are sum of the unbalanced forces and the gas forces.

$$\{F_x\} = \{F_{ux}\} + \{F_{Gx}\} \qquad \{F_y\} = \{F_{uy}\} + \{F_{Gy}\} \tag{20}$$

Equation(19) is numerically integrated to obtain $\{x\}, \{y\}, \{\dot{x}\}$ and $\{\dot{y}\}$ at each time step. The bearing reaction forces $\{F_{Bx}\}$, $\{F_{By}\}$ are obtained by Eq.(13). The origin and the direction of θ are defined as the same as those of ψ. The boundary conditions θ_1, θ_2 are determined where the oil films are ruptured, where pi = 0. Hence, only the active pressure is integrated except for negative pressure. Then, θ_1 and θ_2 cannot be found until the pressure distributions are given, because they vary with time. Hence, the determination of θ_1 and θ_2, and the calculation of $\{F_{Bx}\}$ and $\{F_{By}\}$ are repeated at every time step in the numerical integration. In this analysis, Eq.(19) is integrated by the Runge-Kutta method, and the Simpson's formula is employed for Eq.(13).

Analysis Models and Analytical Conditions

The analysis models of the twin and single rotary compressors are shown in Fig.3. They all have the same discharging capacity. The rotors are supported by three short bearings, S_{B1}, S_{B2} and S_{B3}. Here, the compression gas is sealed between the end of the rolling piston and the bearing flange, and furthermore, both ends of the bearings are usually open through the rotor interior. Therefore, the boundary conditions at the bearing ends where z = 0 and L_i are satisfied. The gas force profiles per rotor revolution, obtained by Eqs.(15) to (18) and used in this analysis, are shown in Fig.4. The dimensions of the balancers are determined

under the static balancing condition on the rotor system. Here, F_{u1}, F_{u2}, F_{G1} and F_{G2}, which act on the two nodes put on the rolling pistons, are divided by 2 to allocate to each node. The models were analyzed at rotor rotating frequency $f_0 = 150$ Hz. The relation among ψ, f_0 and ω is $\psi = 2\pi f_0 = \omega t$. The initial conditions of $\{x\}$, $\{y\}$, etc. were set to zero at $t = 0$, and time integration was performed until the rotor action became steady, namely, 4 revolutions.

RESULTS AND DISCUSSIONS

The rotor actions obtained by this analysis for the twin and single rotary compressors are shown in Fig.5 and Fig.6, respectively. The rotor centers at $\psi = $ 0°, 90°, 180° and 270° are presented in the figures. We can see that the rotors are whirling with bending deformation. Especially, it was found that the deformation and whirling of the motor rotor were large. This was caused by the balancer on the top end of the motor rotor, which was the free end and most distant from S_{B3}. Namely, the motor rotor was bent largely from S_{B3} by the bending moment due to F_{u4}. Comparing (a) with (b) in Fig.5, it is easily seen that the whirling of the twin rotary compressor is smaller for the same rotating speed, because F_{u4} is smaller than that of the single rotary compressor (refer to APPENDIX). The whirling diameters of the top end are 0.12 mm for (a), and 0.24 mm for (b). The rotor action between S_{B1} and S_{B3} is influenced by the bending deformation of the motor rotor, as shown in Fig.6. The rotor is inclined largely between S_{B2} and S_{B3}, and therefore, the eccentricity in S_{B3} is in the opposite direction to the other bearings.

The loci of the rotor center in the bearings are shown in Fig.7. We can see the relative locations of the rotor center in S_{B1}, S_{B2} and S_{B3}, referring to the locations at $\psi = 40°$, 120° and 220°. The loci in S_{B1} and S_{B2} for the twin rotary compressor are smaller than those for the single rotary compressor, and they are only in the negative-x and active-y region. However, the rotor center in S_{B3} is whirling largely by influence of the motor rotor behavior.

Fig.8 shows the profiles of the bearing reaction forces, which are the bearing loads, per rotor revolution. The vertical axis is the compound value of F_{Bxi} and F_{Byi}. For the twin rotary compressor, the load on S_{B1} is the largest except for nearby $\psi = 45°$. On the other hand, for the single rotary compressor, the profiles for S_{B1} and S_{B2} are similar with each other, but the load on S_{B2} is always larger. It can be seen that the gas forces act as loads mainly on S_{B1} and S_{B2} from these characteristics. The load on S_{B3} is small for both compressors. It seems that the load is mainly due to the oil pressure induced by the eccentric rotation of the rotor, as shown in Fig.7. Each peak load is 56.3 kgf on S_{B1} for (a) and 84.2 kgf on S_{B2} for (b), respectively. The bearing loads of the twin rotary compressor are lighter for the same discharging capacity.

Fig.9 shows the variations in the pressure distribution of the oil film in the bearings where $z = 1/2\ L_i$ per rotor revolution. The horizontal axis is the bearing location in the θ direction. The vertical axis is the pressure $p_i - p_a$ for which the origin is displaced at each rotor rotating angle with similar intervals. The pressure in S_{B3}, which transfers in the θ direction with the same phase as ψ, is thus generated on the whole area, because the rotor is whirling along the bearing inner face. The variations in the distributions in S_{B1} and S_{B2} correspond to the bearing load profiles in Fig.8. However, for the single rotary compressor, the pressure induced by the rotor whirl is clearly found in S_{B2} at θ = 180° to 330° and ψ = 0° to 150°. It is the reaction pressure against S_{B3}, as the pressure is in the opposite location to it for S_{B3} at the same rotor rotating angle. Therefore, S_{B2} of the single rotary compressor is loaded by the reaction force of S_{B3} in addition to the gas force. Therefore, it is understood that the load on S_{B2} is larger than that on S_{B1}, as shown in Fig.8(b). For the twin rotary compressor, such a reaction pressure in S_{B2} was not clearly found.

In general, for a rotary compressor, a groove to supply the lubricating oil is prepared on the bearing inner face in the nearly axis direction. This groove is needed to be located where pressure is not generated. By referring to Fig.9(a), it can be seen that the optimum locations of the oil supplying grooves are 180° to 305°, 220° to 290°, and 230° to 330° in S_{B1}, S_{B2} and S_{B3}, respectively, for the twin rotary compressor. The locations for the single rotary compressor are 210° to 300°, 260° to 335°, and 240° to 315°, respectively, from Fig.9(b). Here, the regions of the lower pressures are selected for S_{B3} and S_{B2} of the single rotary compressor.

CONCLUSIONS

The rotor action with elastic bending deformation, the bearing load profiles, and the pressure distributions of the oil film have been obtained, and the differences in the dynamic characteristics between twin and single rotary compressors have been made clear by dynamic analysis. For a twin rotary compressor, the whirling locus and the elastic deformation of the rotor were found to be smaller, and the bearing loads lighter than those of a single rotary compressor with the same discharging capacity, at a high speed drive (at 150 Hz). The optimum locations of the oil supplying groove in the bearing inner face can be determined by referring to the variations of the pressure distributions.

The following properties were used in this analysis.

E (kg/mm^2) : 16500.0
ρ $(kg\ sec^2/mm^4)$: 6.57×10^{-10} (motor rotor)
7.34×10^{-10} (remainder)
c_i (mm) : 0.008
L_i (mm) : 8.0
μ_i (cp) : 3.0 (centipoise)
RB_i (mm) : 16.0 $(i = 1\ to\ 3)$

	(a) Twin Rotary Compressor				(b) Single Rotary Compressor		
j :	1	2	3	4	1	3	4
W_j (Kg) :	0.09	0.09	0.0057	0.0028	0.104	0.054	0.022
r_j (mm) :	3.5	3.5	13.0	13.0	4.02	13.0	13.0
ϕ_{uj}(deg.) :	0	180	180	0	0	180	0

	Upper	Lower	
r :	1.15	1.15	1.15
R_r (mm) :	16.55	16.55	16.03
R_c (mm) :	20.05	20.05	20.05
h_c (mm) :	16.0	16.0	28.0
$p_s(kg/mm^2)$:	0.06	0.06	0.06
$p_d(kg/mm^2)$:	0.23	0.23	0.23

.

REFERENCES

(1) Przemieniecki.J.,S.
"Theory of Matrix Structural Analysis", McGraw-Hill, 1968

(2) Pandeya,P.,Soedel,W.
"Rolling Piston Type Rotary Compressors with Special Attention to Friction and Leakage", 1978 PURDUE, Compressor Technology Conference, 1978.1
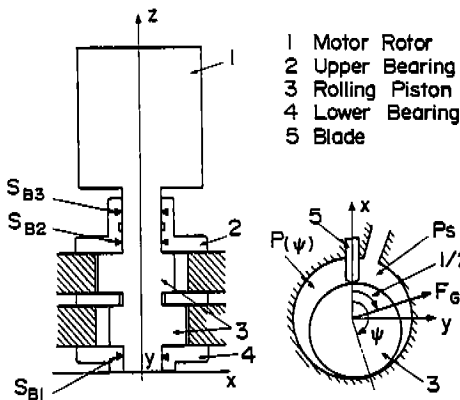
Fig.1 Rotor-Journal Bearing System and Compression Unit of Twin Rotary Compressors
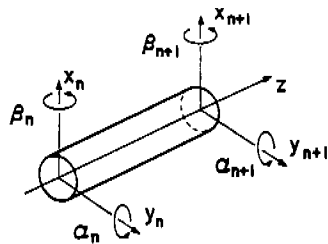
Fig.2 Local Coordinate System of Beam Elements
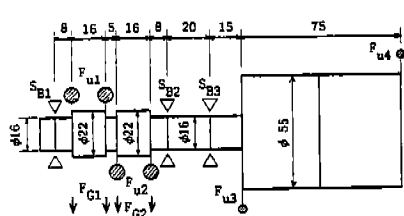
(a) Twin Rotary Compressor
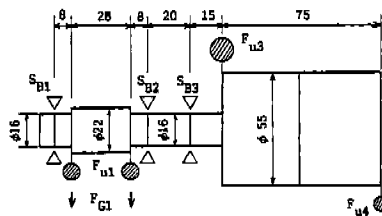
(b) Single Rotary Compressor

Fig.3 Analysis Models
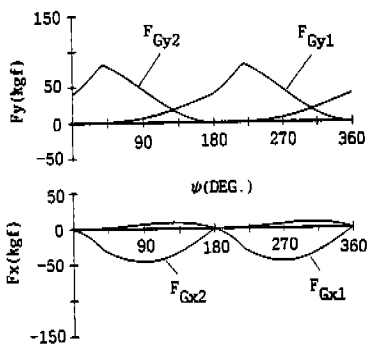
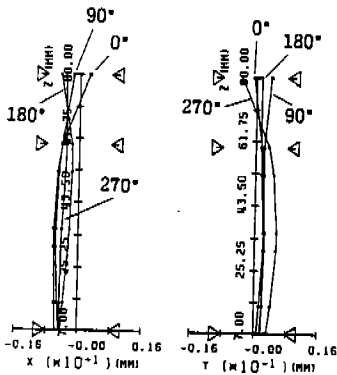(a) Twin Rotary Compressor
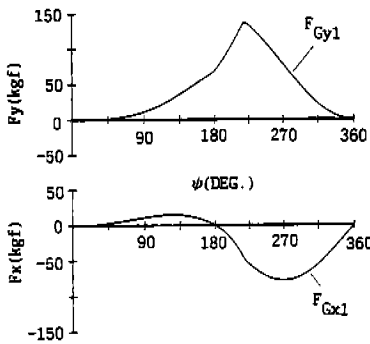
(b) Single Rotary Compressor

Fig.4 Gas Forces
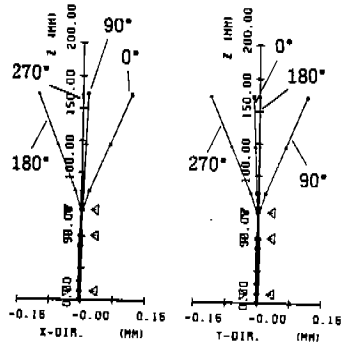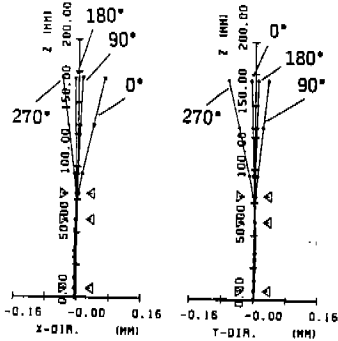
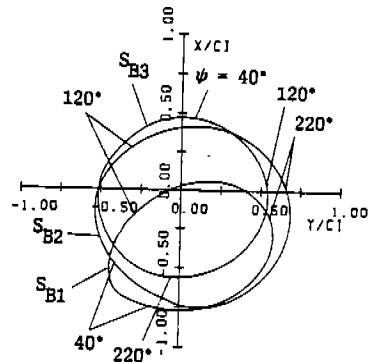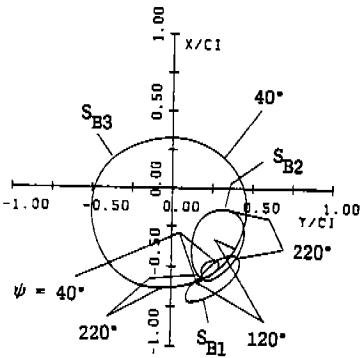(a) Twin Rotary Compressor   (b) Single Rotary Compressor

Fig.5 Rotor Actions
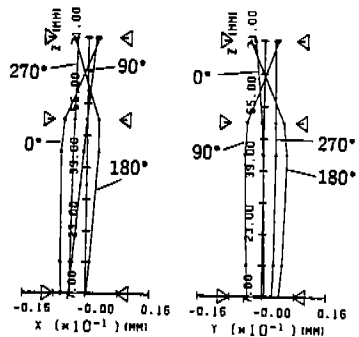
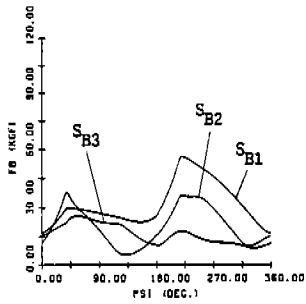(a) Twin Rotary Compressor   (b) Single Rotary Compressor

Fig.6 Rotor Actions Between Bearings

(a) Twin Rotary Compressor   (b) Single Rotary Compressor
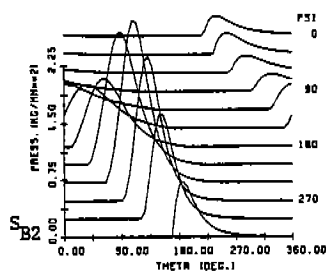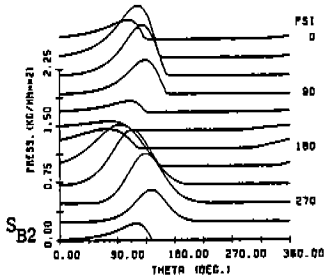
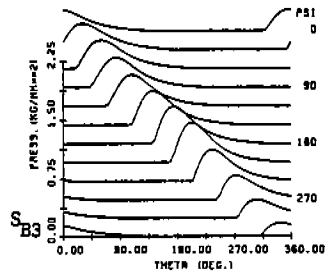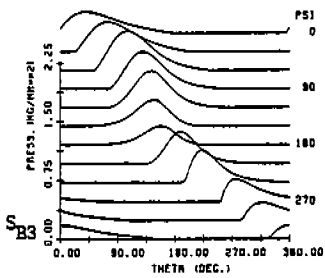Fig.7 Loci of Rotors in Bearings

759
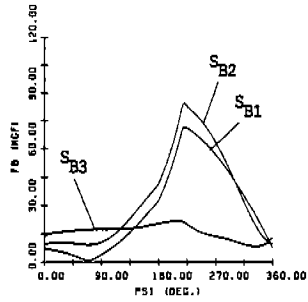
(a) Twin Rotary Compressor   (b) Single Rotary Compressor

Fig.8 Bearing Load Profiles
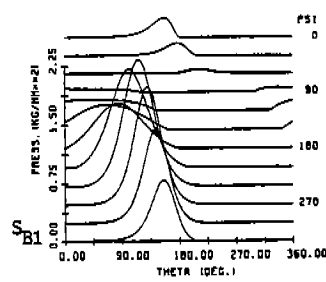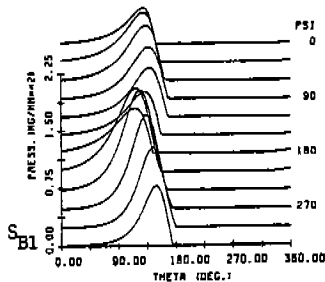
(a) Twin Rotary Compressor   (b) Single Rotary Compressor

Fig.9 Pressure Distributions of Oil Films